Journal of Biomechanics 45 (2012) 2884–2892

Contents lists available at SciVerse ScienceDirect

Journal of Biomechanics

journal homepage: www.elsevier.com/locate/jbiomech
www.JBiomech.com

A new approach to determine the accuracy of morphology–elasticity relationships in continuum FE analyses of human proximal femur

Javad Hazrati Marangalou, Keita Ito, Bert van Rietbergen *

Orthopaedic Biomechanics, Biomedical Engineering Department, Eindhoven University of Technology, Eindhoven, The Netherlands

ARTICLE INFO

Article history:
Accepted 5 August 2012

Keywords:
Continuum-level finite elements method
Micro-finite elements method
Anisotropy
Proximal femur

ABSTRACT

Continuum finite element (FE) models of bones are commonly generated based on CT scans. Element material properties in such models are usually derived from bone density values using some empirical relationships. However, many different empirical relationships have been proposed. Most of these will provide isotropic material properties but relationships that can provide a full orthotropic elastic stiffness tensor have been proposed as well. Presently it is not clear which of these relationships best describes the material behavior of bone in continuum models, nor is it clear to what extent anisotropic models can improve upon isotropic models. The best way to determine the accuracy of such relationships for continuum analyses would be by quantifying the accuracy of the calculated stress/strain distribution, but this requires an accurate reference distribution that does not depend on such empirical relationships. In the present study, we propose a novel approach to generate such a reference stress distribution. With this approach, stress results obtained from a micro-FE model of a whole bone, that can represent the bone trabecular architecture in detail, are homogenized and the homogenized stresses are then used as a reference for stress results obtained from continuum models. The goal of the present study was to demonstrate this new approach and to provide examples of comparing continuum models with anisotropic versus isotropic material properties.

Continuum models that implemented isotropic and orthotropic material definitions were generated for two proximal femurs for which micro-FE results were available as well, one representing a healthy and the other an osteoporotic femur. It was found that the continuum FE stress distributions calculated for the healthy femur compared well to the homogenized results of the micro-FE although slightly better for the orthotropic model ($r=0.83$) than for the isotropic model ($r=0.79$). For the osteoporotic bone also, the orthotropic model did better ($r=0.83$) than the isotropic model ($r=0.77$). We propose that this approach will enable a more relevant and accurate validation of different material models than experimental methods used so far.

1. Introduction

Continuum finite element (FE) analysis has become a standard computational tool for the analysis of bone mechanical behavior in orthopedic biomechanics. It is commonly used to evaluate bone loading conditions, e.g. after the placement of implants (Huiskes, 1993; Huiskes and Chao, 1983; Pettersen et al., 2009; Weinans et al., 2000) and to evaluate bone strength e.g. in case of osteoporosis or drug treatments (Chevalier et al., 2010; Guo and Kim, 2002; Tawara et al., 2010; Verhulp et al., 2008). Patient-specific finite element models are usually generated based on clinical CT scans. From such scans, the geometry as well as the bone density distribution can be easily derived. Empirical relationships are then needed to calculate bone material parameters from the measured density distribution.

Many different empirical relationships have been described in the literature. With the more simple ones, bone is modeled as isotropic and a power law relationship is used to calculate the isotropic Young's modulus from the bone density (Carter and Hayes, 1976; Keller, 1994; Keyak et al., 1994, 1997; Morgan et al., 2003; Rice et al., 1988). It is known, however, that cancellous bone can be highly anisotropic. More advanced relationships that can describe the full anisotropic elastic behavior of cancellous bone have been developed as well. With such relationships, bone elastic behavior is usually described as orthotropic with the principal orthotropic axes determined by the underlying micro-architecture and some power law to calculate the values of the orthotropic elastic constants. In this case also, several different orthotropic relationships have been developed (Cowin, 1985; Cowin and Turner, 1992; Kabel et al.,

* Correspondence to: Eindhoven University of Technology, Biomedical Engineering Department, Orthopaedic Biomechanics, PO Box 513, GEM-Z 4.118, 5600, MB Eindhoven, The Netherlands. Tel.: +31 40 247 4773; fax: +31 40 247 3744.
E-mail address: B.v.Rietbergen@tue.nl (B. van Rietbergen).

0021-9290
http://dx.doi.org/10.1016/j.jbiomech.2012.08.022

1999b; Turner et al., 1990; Yang et al., 1998; Zysset and Curnier, 1995). In these relationships, the orientation of the trabeculae is usually quantified by a second rank fabric tensor which represents the average trabecular orientation (Harrigan and Mann, 1984; Odgaard, 1997). Since this can be difficult or impossible to measure from clinical CT scans, it has been proposed as well to base the trabecular orientation on the anatomical site (Yang et al., 1998).

It presently is unclear which relationship would provide the best results for continuum FE analyses of whole bones. Moreover, it is even unclear to what extent the use of such more advanced anisotropic relationships would improve the accuracy of the finite element calculations over more simple isotropic models.

In order to test the accuracy of different isotropic or anisotropic relationships for modeling material properties in continuum FE analyses, a 'gold standard' is required relative to which the results of the analyses can be tested. So far, experimental test on whole bones have been used as a reference (Chevalier et al., 2008; Keyak et al., 1993; Pahr and Zysset, 2009; Taddei et al., 2006; Trabelsi et al., 2011). For whole bones, however, experimental results are usually limited to surface strain measurements and to measurement of the stiffness of the whole bone. Based on such measurements, it is not possible to validate the stress or strain distribution within the cancellous bone tissue, which is the most important region for implant fixation. Also, the surface strains and total bone stiffness obtained from FE models might not be very sensitive to the choice of the empirical constants, as long as the cortical bone stiffness is well represented, nor to the choice of an isotropic versus an anisotropic model for the cancellous bone.

In the present study, we propose another approach to test the accuracy of different empirical material laws for continuum FE analyses of bone. With this approach, results obtained from a micro-FE model of a whole bone that can represent the bone trabecular architecture in detail are used as a reference (Fig. 1). Such micro-FE models thus account for the effect of the bone density and anisotropy that result from the bone micro-architecture without the need for any empirical relationships. The stresses and strains obtained from such models are those at the level of the bone tissue, but after homogenization of these stresses and strains they can be directly compared to those obtained from continuum FE models. The difference between the standard approach to calculate the continuum level stress distribution and the approach that we take here to generate a 'gold standard' is depicted in Fig. 1. With the standard approach, the bone micro-architecture is homogenized to a density and fabric value, and a continuum FE model is created with material properties based on these homogenized values. With the approach that we take here, a micro-FE model is used to calculate bone tissue level stresses and strains and the results are homogenized.

The goal of the present study was to demonstrate this new approach by comparing the calculated stress distributions in a continuum model of a healthy and an osteoporotic femur, implementing isotropic and anisotropic material properties, with homogenized micro-FE results of the same bones.

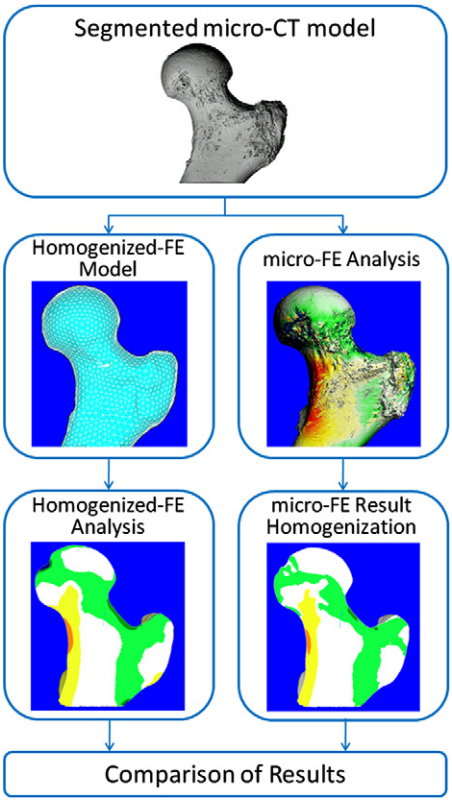

Fig. 1. Design of the study; results of a continuum-level FE model that incorporates the material law to be tested (left) are compared to homogenized micro-FE results that are taken as the gold standard (right).

2. Materials and methods

2.1. Samples

Two human proximal femurs, a healthy femur and a severely osteoporotic femur collected for an earlier study (van Rietbergen et al., 2003), were used. These femurs were scanned using a micro-CT scanner (micro-CT80; Scanco, Brüttisellen, Switzerland) at a resolution of 80 μm, covering a length of approximately 92 mm of each femur. After scanning, a thresholding algorithm was applied to separate the bone from the marrow phase. More information about the samples and scanning procedure can be found in van Rietbergen et al. (2003).

2.2. Creation of continuum-FE meshes

Continuum finite element models of proximal femurs were generated based on contours of the bone periosteal surface that were generated semi-automatically using the software provided with the micro-CT scanner. Using a marching cubes algorithm on the volume comprised by these contours, a triangularization of the bone surface was obtained. This surface was converted to STL format and imported into ANSYS 12.1 (Ansys, Inc., United States) for volumetric meshing. Meshing was done using tetrahedron elements with a typical size of 2 mm.

2.3. Calculation of homogenized material properties

In order to calculate anisotropic material properties, an element density and fabric tensor were calculated for each element. This was done using a semi-automatic mapping algorithm. In the first step; the femur was separated into two compartments: a cortical and a cancellous one using the software provided with the micro-CT scanner (IPL, Scanco Brüttisellen, Switzerland). A minimum of 1 mm cortical thickness was assumed near bone external surfaces. Using an in-house developed algorithm, the type (cortical or cancellous) and number of voxels within each element were determined. For each element, fully or partially within the cancellous compartment, a spherical VOI around the element center with a radius of 2 mm was defined. For each VOI, bone volume fraction (BV/TV) and mean intercept length (MIL) based fabric tensor were determined and assigned to the element, considering only the region in the cancellous compartment. For elements fully or partly in the cortical compartment, a cortical volume fraction was defined considering only the region within the cortical compartment and an identity tensor was specified as the fabric tensor. As an example, a contour band plot of the calculated bone volume fraction (ρ) and a vector plot of the fabric main direction (largest eigen-value after normalization) for the osteoporotic and healthy femurs are shown in Fig. 2.

Based on the element density ρ and fabric tensor $\mathbf{M}$, the element compliance tensor $\mathbb{C}$ was calculated using the fabric–elasticity relationship of Zysset and Curnier (Zysset, 2003; Zysset and Curnier, 1995):

$$\mathbb{C} = \sum_{i=1}^{3} \frac{1}{\varepsilon_0 \rho^k m_i^{2l}} \mathbf{M}_i \otimes \mathbf{M}_i - \sum_{i,j=1;i\neq j}^{3} \frac{v_0}{\varepsilon_0 \rho^k m_i^l m_j^l} \mathbf{M}_i \otimes \mathbf{M}_j + \sum_{i,j=1;i\neq j}^{3} \frac{1}{2G_0 \rho^k m_i^l m_j^l} \mathbf{M}_i \overline{\otimes} \mathbf{M}_j \quad (1)$$

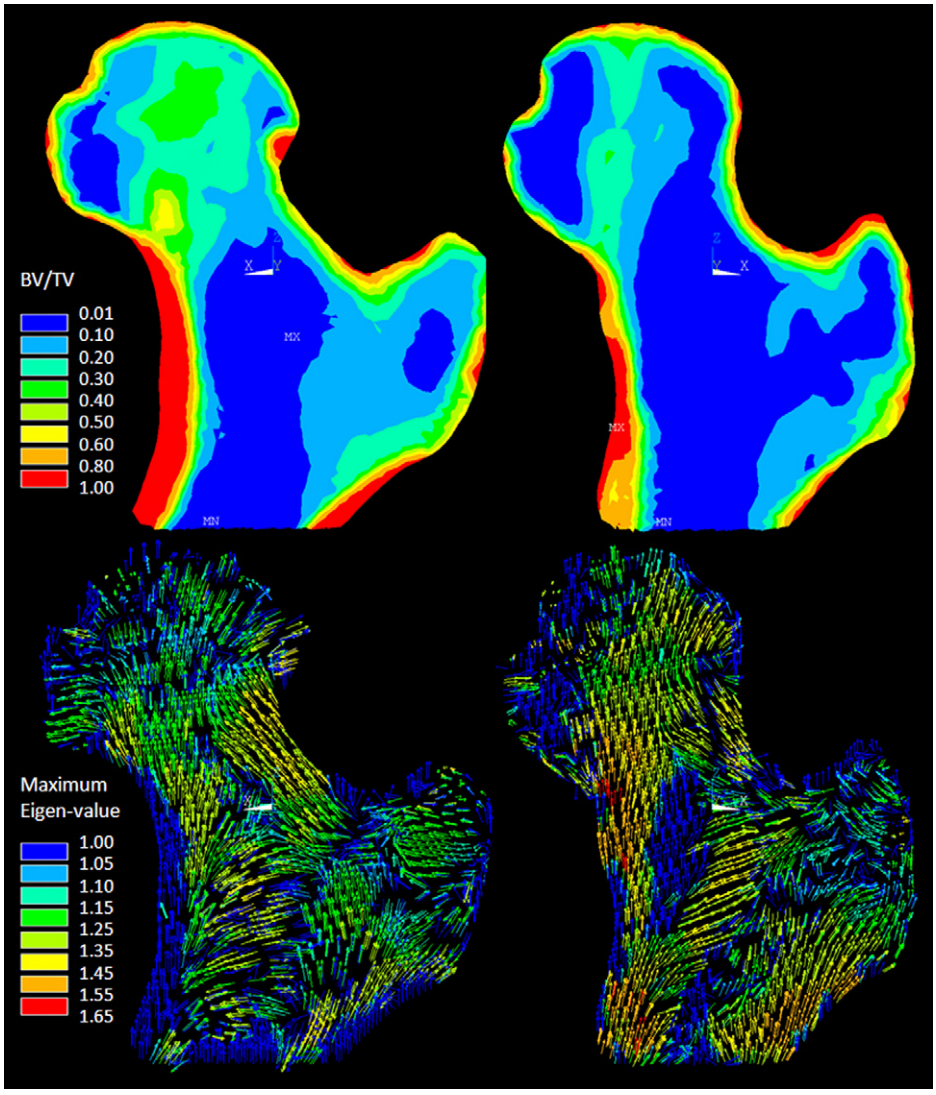

Fig. 2. Bone morphological parameters; bone volume fraction and main direction (eigen-values normalized to have $Tr(M)=3$, where M is the fabric tensor) for healthy (left) and osteoporotic (right) femurs.

Table 1
Constants used in the Zysset–Curnier relationship.

ε_0 (GPa)]	v_0	G_0 (GPa)	k	l
22.5	0.3	8.65	1.914	1

ε_0, v_0, G_0 are elastic constants, m_i the normalized eigen-values and $\mathbf{M_i}$ the dyadic product of the eigenvectors of fabric tensor $\mathbf{M}$:

$$\mathbf{M}=\sum_{i=1}^{3} m_i\mathbf{M}_i=\sum_{i=1}^{3} m_i(m_i\otimes m_i),\quad Tr(\mathbf{M})=3, \tag{2}$$

In the case of modeling isotropic material properties, the fabric tensor is simply replaced by the identity tensor. The elastic constants (Table 1) were scaled to be in agreement with Young's moduli used for micro-FE analyses (Verhulp et al., 2006). For elements that cover both compartments, a mixture rule was used to calculate a stiffness tensor that is a mixture of the cancellous and cortical stiffness tensor, using the element cancellous and cortical bone fraction as scaling factors.

2.4. Homogenization of micro-FE results

As mentioned earlier, micro-FE results obtained for the same femurs (Verhulp et al., 2008) were taken as the gold standard. Using the same meshes as used for the continuum model, an averaging technique was used to homogenize the bone tissue stress tensors over the element volumes. This averaging should be performed over the total element volume, V_{tot}, comprising the voxels that represent both bone tissue and those that represent the marrow region. In the micro-FE model, however, stress and strain values were calculated only for the voxels representing bone tissue V_{tissue}. Since the stresses in the other voxels (representing bone marrow) are zero anyway, the homogenized stress $\overline{\sigma}$could be calculated by integrating the tissue stress tensors σ over the bone tissue volume only

$$\overline{\sigma}=\frac{1}{V_{tot}}\int \sigma dV_{tot}=\frac{1}{V_{tot}}\int \sigma\, dV_{tissue} \tag{3}$$

After calculating the homogenized stress tensor for each element, the homogenized principal stress values were calculated.

2.5. Boundary conditions

The boundary conditions applied were chosen to be the same in the continuum and micro-FE model and represented loading conditions typically applied in an experimental setting to simulate a fall-on-the-side situation (Cheng et al., 1997; Courtney et al., 1994, 1995). In this setup the angle between the vertical and the shaft axis was 10° and the femur was internally rotated by 15°. The load magnitude was 1 kN, distributed over the femoral head. The individual nodal forces were directed toward the center of the femoral head to represent loading conditions expected when a frictionless cartilage layer is present. The nodes on the surface of the trochanter, in a 5 mm layer perpendicular to the resultant hip force, were fixed in the vertical direction and the nodes on the distal end of the femur were constrained in the horizontal direction (Fig. 3).

2.6. Comparison of results

Contour and vector plots of the largest principal stress component were made for a qualitative comparison of the stress distribution obtained from the continuum model and from the homogenized micro-FE results. For a quantitative comparison, the homogenized micro-FE principal stress values for elements in the neck region were correlated with those of the continuum models and a Pearson's linear correlation coefficient was calculated based on an element by element value comparison. Only elements in the femoral neck were selected since this is the most critical region for loading condition as applied here and since it is sufficiently far away from the regions where boundary conditions were applied, thus avoiding errors due to the close proximity of external constraints.

Furthermore, the whole bone stiffness was calculated and compared for all models. Since in all models the applied load was distributed over a large number of nodes, it was not possible to define a meaningful deflection of the bone when loaded. Instead, an energy-equivalent deflection d was calculated from the energy equation:

$$\frac{1}{2}Fd = \int U\,dV \tag{4}$$

with F the applied force and U the strain energy density. Using this deflection d, the stiffness k then was calculated as

$$k = \frac{F}{d} = \frac{F^2}{2\int U\,dV} \tag{5}$$

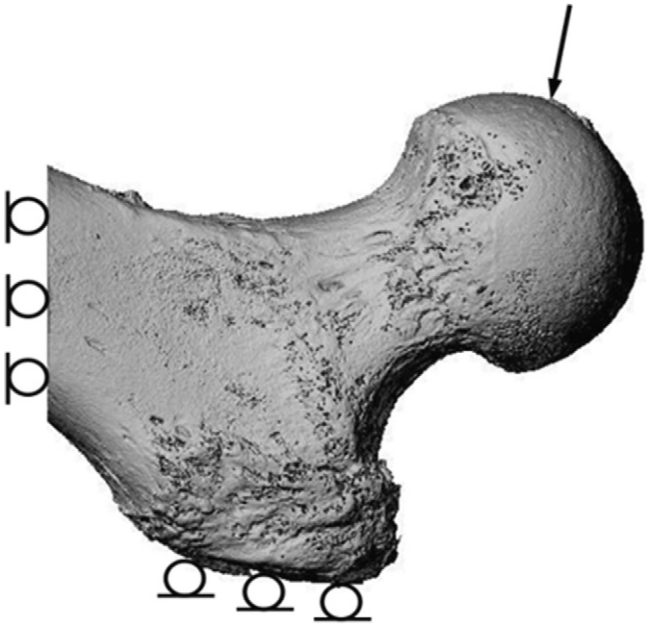

Fig. 3. Applied boundary conditions to FE models; the arrow represent resultant hip force.

3. Results

Contour plots of the homogenized principal stress values are shown in Fig. 4. These plots serve as the gold standard relative to which the results of the continuum FE will be compared. Contour plots of the largest principal stress component in the healthy and osteoporotic femur as obtained from the continuum models are depicted in Fig. 5. It can be seen that the stress distributions obtained from the continuum models are both qualitatively and quantitatively very similar to those obtained from the micro-FE results. The most notable difference is the somewhat higher stress values at the distal side of the femoral neck and the proximal side of the femoral head in the continuum models. The latter is likely

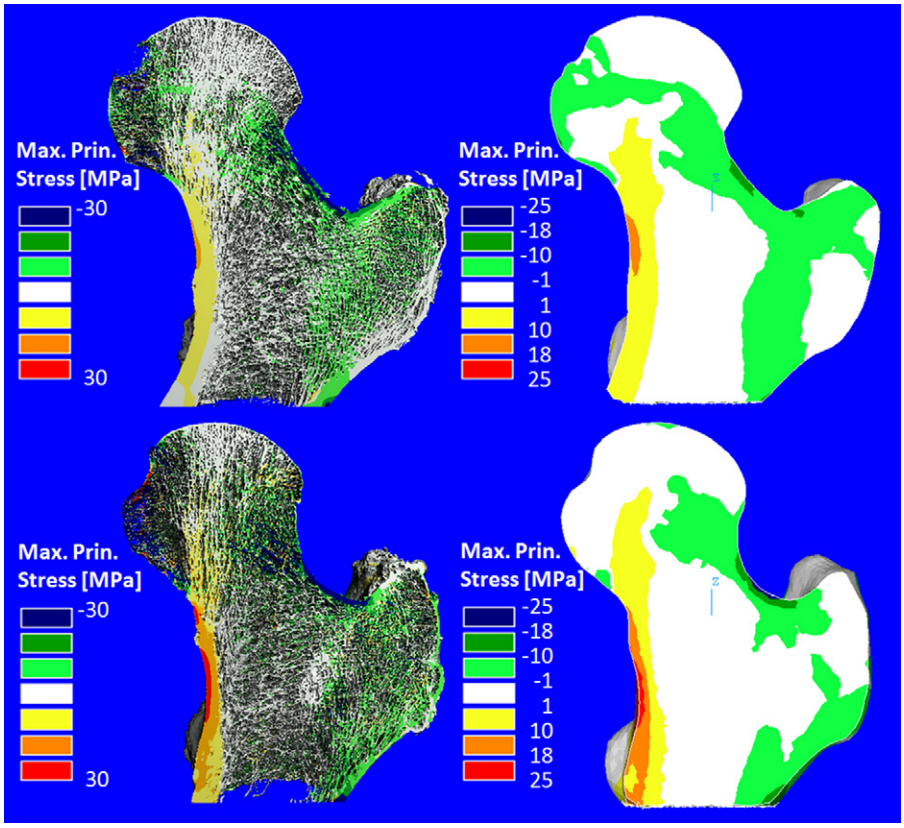

Fig. 4. Micro-FE results and homogenized micro-FE results; maximum principal stress (MPa) distributions in the micro-FE models (Verhulp et al., 2008) and homogenized distributions in the continuum-FE models for the healthy (top) and osteoporotic (bottom) femurs.

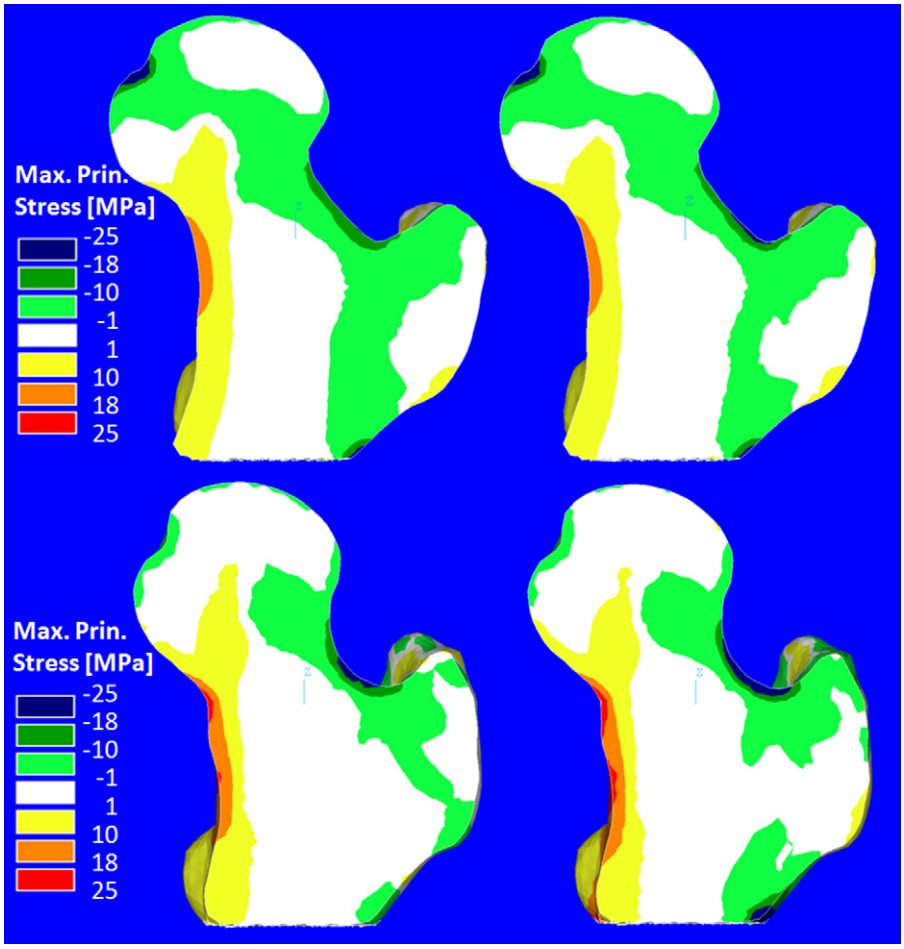

Fig. 5. Top: maximal principal stress (MPa) distribution for the healthy femur, calculated using the orthotropic continuum model (left) and the isotropic continuum model (right). Bottom: the same for the osteoporotic femur.

an effect of the applied boundary conditions. For the isotropic models a comparison of the stress distribution in the continuum FE and homogenized micro-FE models resulted in a correlation coefficient $r=0.798$ for the healthy model and $r=0.773$ for the osteoporotic model. For the orthotropic models, a correlation coefficient $r=0.831$ was found for the healthy femur and $r=0.830$ for the osteoporotic one (Fig. 6).

Contour plots of the strain energy density distribution (Fig. 7) showed very similar results as the maximum principal stress plots. In particular for the osteoporotic femur, the orthotropic model better compared to the micro-FE results than the isotropic model.

To get a better insight in the differences between the results of continuum and homogenized micro-FE stresses, we also plotted the relative error in the maximum principal stress calculation obtained from the isotropic model when compared to the gold standard for the healthy femur versus the bone volume fraction (Fig. 8). From this result, it is clear that the larger errors are found in regions with low bone volume fraction.

In order to visualize the correspondence in the directions of the maximum principal stress component, vector plots of the maximum principal stress are shown in Fig. 9. The vector plots from continuum models compare qualitatively well with the ones from micro-FE models. In particular for the osteoporotic femur it can be seen that at some locations (notably Ward's triangle) the agreement is less favorable.

The results for the whole bone stiffness are shown in Table 2; from these results it can be seen that the continuum models tend to overestimate the stiffness, in particular when using isotropic material properties. For the healthy femur, this overestimation was 10% for the orthotropic model and 14% for the isotropic model. For the osteoporotic femur, the same overestimation was found for orthotropic model, but for the isotropic model the stiffness was overestimated by as much as 52%.

4. Discussion

The goal of this study was to demonstrate a new approach to evaluate the accuracy of the stress distributions calculated from continuum FE models that implement different material models. The material model used in this study was either an isotropic one based on the density distribution or an orthotropic one, based on bone density and fabric using a relationship proposed in the literature (Zysset and Curnier, 1995). This new approach uses homogenized micro-FE stress distributions as the gold standard relative to which the results of the continuum models can be compared.

We found good agreement between results obtained from the homogenized micro-FE models and those of the continuum models. This indicates that bone density, or a combination of bone density and fabric, in combination with the material models chosen well represents the mechanical properties of cancellous bone. For the two bones investigated here, the orthotropic models provided slightly more accurate results than isotropic models. These results are in accordance with earlier studies where orthotropic models improved the predictions of vertebral body apparent stiffness

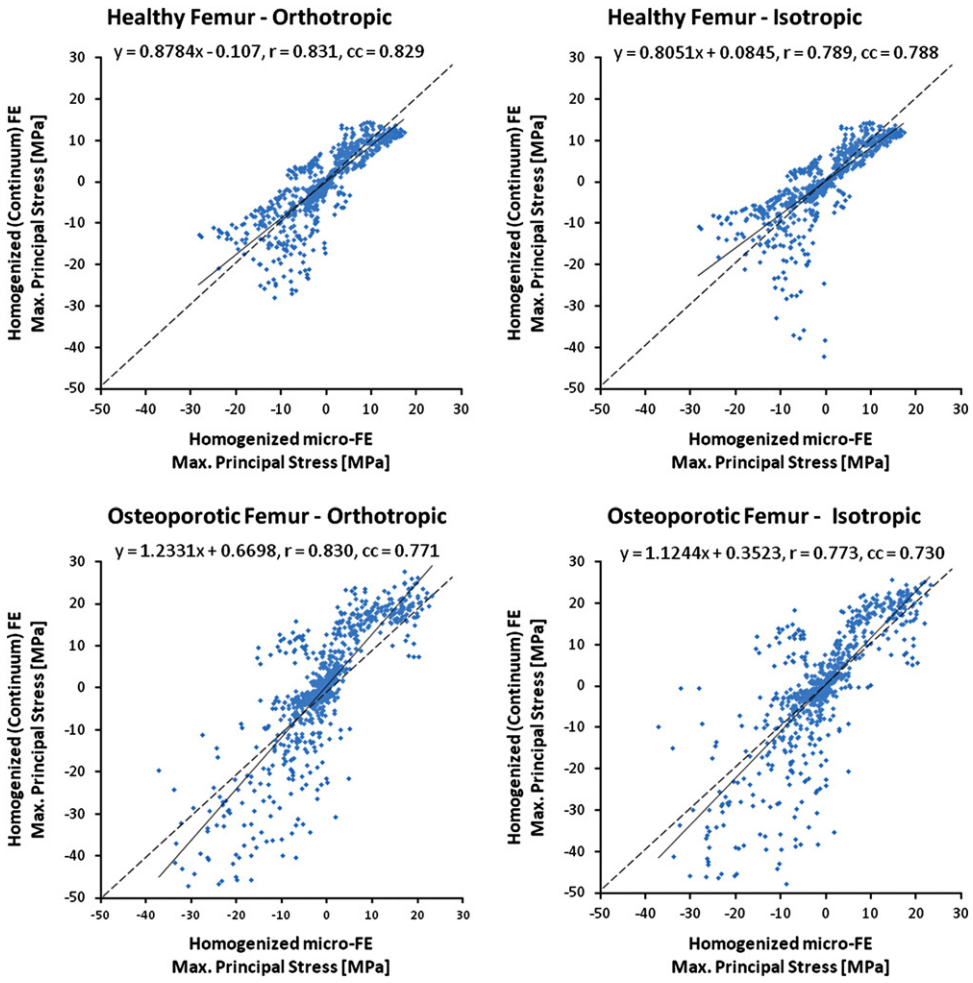

Fig. 6. Regression of micro-FE and continuum-FE predicted results based on isotropic and orthotropic material properties for the healthy (upper panels) and osteoporotic (bottom panels) bone (r: linear correlation coefficient and cc: concordance correlation coefficient).

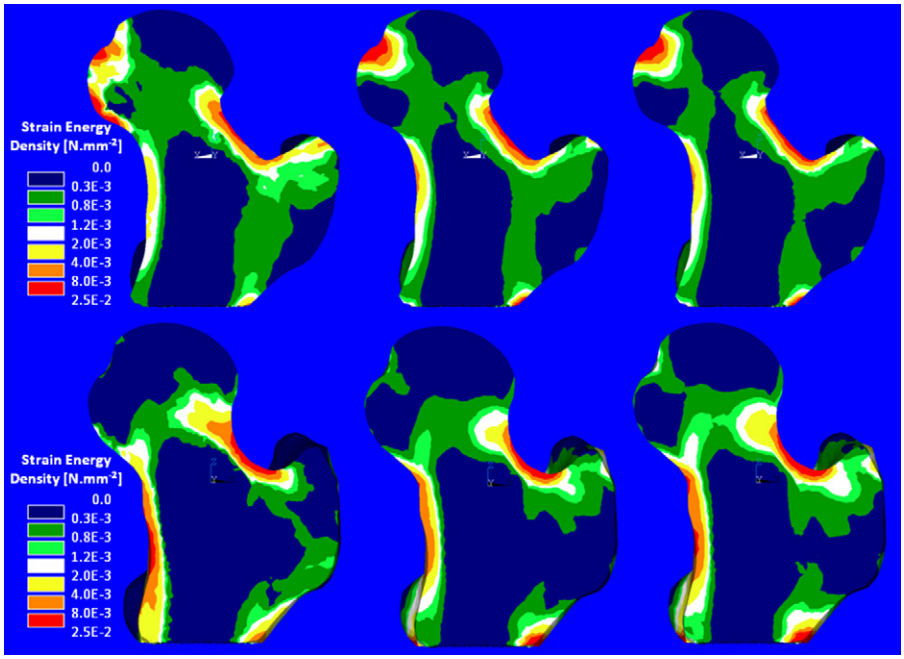

Fig. 7. Strain energy density (SED) plots for homogenized micro-FE (left), orthotropic (middle) and isotropic (right) models within healthy femur (top) and osteoporotic femur (bottom).

with respect to isotropic models (Pahr and Zysset, 2009). The osteoporotic bone benefited more from an orthotropic material description than the healthy bone model. However, a thorough comparison between the accuracy of isotropic and orthotropic models is not possible due the limitations in the number of the samples used in this study.

In the present study we could use micro-CT images of the bones for the measurement of the element fabric tensor. When only clinical CT data is available, this is not possible since the resolution of such images is not good enough to resolve the trabecular architecture required to measure fabric. Nevertheless, methods have been developed to obtain at least some indication of the bone fabric even from clinical CT images (Tabor, 2007). Recently developed high resolution flat-panel CT scanning techniques might provide a resolution that is good enough to determine fabric of trabecular bone even in-vivo (Bredella et al., 2008; Cheung et al., 2009; Gupta et al., 2006; Walsh et al., 2010). Although in most of these studies only bone in the peripheral skeleton was considered, applications to the spine and femur have been reported as well (Mulder et al., 2012). In case no patient-specific information about the fabric can be obtained, using a generalized fabric direction might be a possible solution as well.

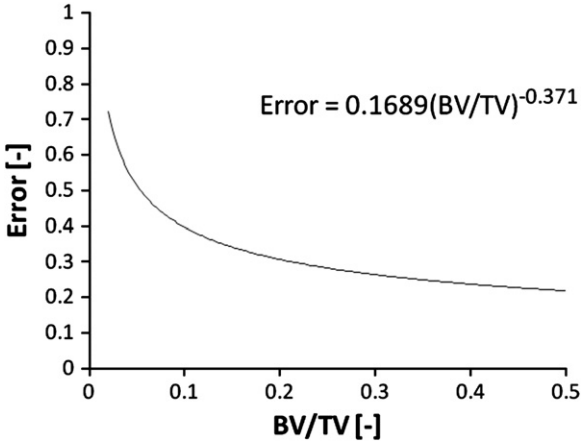

Fig. 8. Relative error in the maximum principal stress magnitude in the isotropic model for the healthy femur.

The present study focused on the accuracy of only the stress distribution. The accuracy of the strain distribution was not investigated. The reason for this is that for the homogenization of the micro-FE calculated strains the strains in the marrow region also are needed. Unlike for the stresses, the strains in these regions are not zero and Eq. (3) cannot be used for strains. Since the marrow region was not meshed in the micro-FE models, it was not possible to apply a proper homogenization of the micro-FE calculated strains. It is possible though, to compare the strains for the continuum models that implement isotropic and anisotropic material properties. Fig. 10 shows the maximum principal strain distribution for all continuum models. It can be seen that the strain distributions in the isotropic and orthotropic models are very similar, although strains in the isotropic model are slightly higher than those in the anisotropic model.

Although in this study we have compared the whole-bone stiffness, we did not compare the elastic properties of the elements in the continuum models to the elastic stiffness of the corresponding regions in the micro-FE models. The reason for this is twofold. First, most bone morphology–stiffness relationships have already been well validated by comparing elastic properties calculated from the morphology parameters with those measured in experiments or from micro-FE analyses of the same specimens (Matsuura et al., 2008; Rincon-Kohli and Zysset, 2009). Second, although it would be theoretically possible to calculate the

Table 2
Stiffness calculated for the different models (N/mm).

	Micro-FE	Orthotropic	Isotropic
Healthy	3865.967	4263.505 (+10%)	4406.971 (+14%)
Osteoporotic	2643.209	2915.581 (+10%)	4025.246 (+52%)

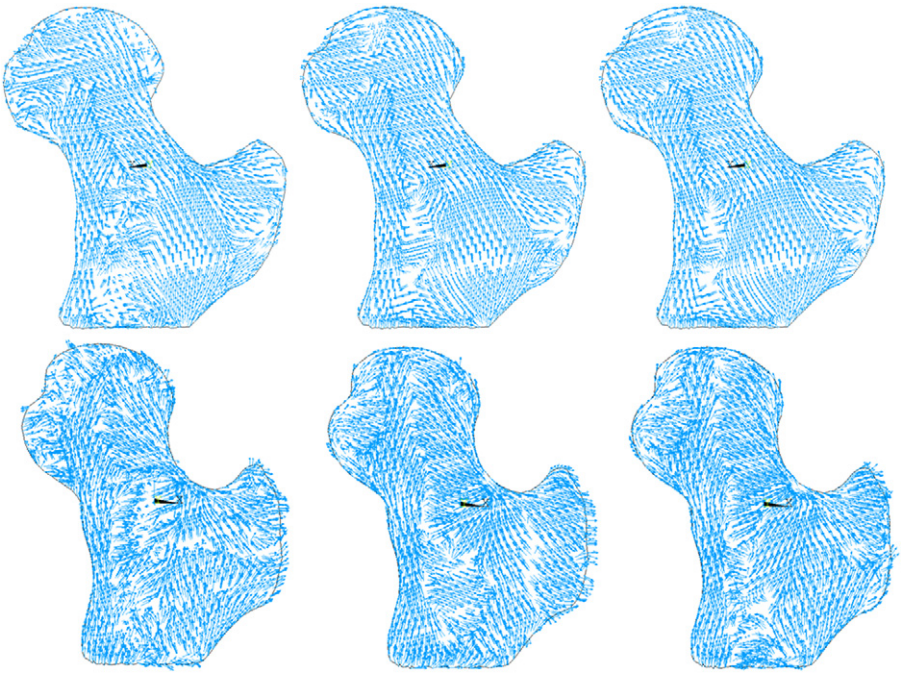

Fig. 9. Maximum principal stress vector plots for micro-FE (left), orthotropic (middle) and isotropic (right) models for the healthy femur (top) and osteoporotic one (bottom).

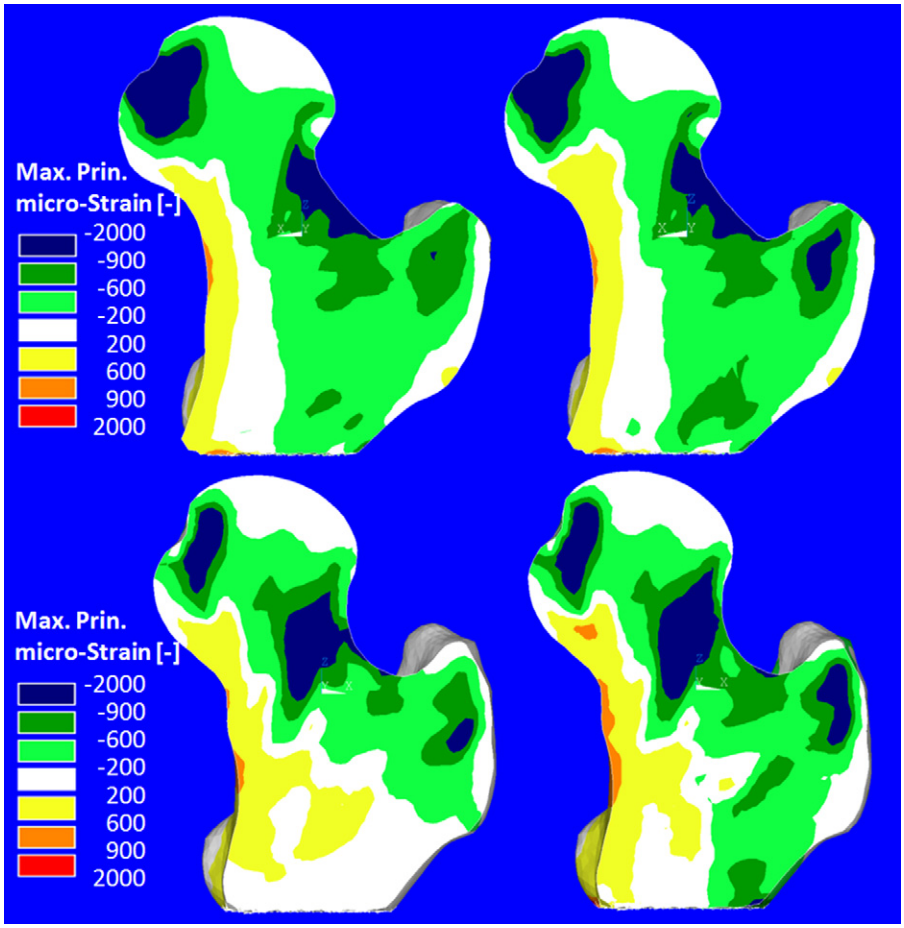

Fig. 10. Top: maximal principal strain [-] distribution for the healthy femur, calculated from the orthotropic continuum model (left) and the isotropic continuum model (right). Bottom: the same for the osteoporotic femur.

stiffness of the spherical region around each element based on micro-FE results, this would be extremely expensive and was out-of the scope of the present study.

Some other limitations of this study must be mentioned as well. First, we analyzed only two femurs and only two material models. However, our main goal was to test the new approach, and the results provided here should be considered merely as a demonstration. Second, we applied only one set of loading conditions. We selected loading conditions representing a fall because we expected that stresses and strains during non-physiological loading conditions might be more sensitive to the material model used than those during physiological loading conditions. The reason for this expectation is that, if bone is adapted to physiological loading conditions, the highest stress and strain values are expected in the principal anisotropic direction. In that case the stiffness in only that principal direction is of importance, whereas the stiffness in the transversal directions hardly plays a role. During non-physiological loading, however, high stresses and strains are expected also in transversal directions.

It should be noted as well that the exact way, in which the bone density and fabric (from which the elastic properties in the continuum model were derived) are determined, could also have an effect on the results. In the present study we defined a spherical volume with a radius of 2 mm around the element centroid for calculation of the element density and fabric. This choice was based on the notion that, in order to define valid continuum level properties, measurements over a length scale on the order of 4 mm are required (Harrigan et al., 1988). Setting this radius to a larger or smaller value will slightly change the results, and thus the material properties in the continuum model. To test the sensitivity of the results to the radius size, we performed a pilot study in which the radius was varied from 2 mm to 8 mm. The results showed that the actual chosen size has a very small effect on the calculated bone volume fraction, fabric tensor and degree of anisotropy. Our choice of the fabric tensor used (MIL) was based on the fact that it was the tensor that was used when the orthotropic material models were defined. Selecting other fabric tensors, however, will likely not affect the results much (Kabel et al., 1999a).

In conclusion, we have demonstrated that a micro-FE stress/strain homogenization procedure can be used as a reference relative to which results of continuum models can be compared to evaluate the accuracy of the models. We propose that this approach will enable a more relevant and accurate validation of different material models than experimental methods used so far.

Conflict of interest statement

We declare that there are no issues that may be considered as potential conflicts of interest to this work.

Acknowledgments

Funding from the European Union for the Osteoporotic Virtual Physiological Human Project (VPHOP FP7-ICT2008-223865) is gratefully acknowledged.

References

Bredella, M.A., Misra, M., Miller, K.K., Madisch, I., Sarwar, A., Cheung, A., Klibanski, A., Gupta, R., 2008. Distal radius in adolescent girls with anorexia nervosa: trabecular structure analysis with high-resolution flat-panel volume CT1. Radiology 249, 938–946.

Carter, D.R., Hayes, W.C., 1976. Bone compressive strength: the influence of density and strain rate. Science 194, 1174–1176.

Cheng, X.G., Lowet, G., Boonen, S., Nicholson, P.H.F., Brys, P., Nijs, J., Dequeker, J., 1997. Assessment of the strength of proximal femur in vitro: Relationship to femoral bone mineral density and femoral geometry. Bone 20, 213–218.

Cheung, A., Bredella, M., Al Khalaf, M.M., Grasruck, M., Leidecker, C., Gupta, R., 2009. Reproducibility of trabecular structure analysis using flat-panel volume computed tomography. Skeletal Radiology 38, 1003–1008.

Chevalier, Y., Pahr, D., Zysset, P.K., 2008. Anatomy- and morphology-based smooth finite element models of the vertebral body. Journal of Biomechanics 41 S252–S252.

Chevalier, Y., Quek, E., Borah, B., Gross, G., Stewart, J., Lang, T., Zysset, P., 2010. Biomechanical effects of teriparatide in women with osteoporosis treated previously with alendronate and risedronate: results from quantitative computed tomography-based finite element analysis of the vertebral body. Bone 46, 41–48.

Courtney, A.C., Wachtel, E.F., Myers, E.R., Hayes, W.C., 1994. Effects of loading rate on strength of the proximal femur. Calcified Tissue International 55, 53–58.

Courtney, A.C., Wachtel, E.F., Myers, E.R., Hayes, W.C., 1995. Age-related reductions in the strength of the femur tested in a fall-loading configuration. Journal of Bone and Joint Surgery 77, 387–395.

Cowin, S.C., 1985. The relationship between the elasticity tensor and the fabric tensor. Mechanics of Materials 4, 137–147.

Cowin, S.C., Turner, C.H., 1992. On the relationship between the orthotropic Young's moduli and fabric. Journal of Biomechanics 25, 1493–1494.

Guo, X.E., Kim, C.H., 2002. Mechanical consequence of trabecular bone loss and its treatment: a three-dimensional model simulation. Bone 30, 404–411.

Gupta, R., Grasruck, M., Suess, C., Bartling, S., Schmidt, B., Stierstorfer, K., Popescu, S., Brady, T., Flohr, T., 2006. Ultra-high resolution flat-panel volume CT: fundamental principles, design architecture, and system characterization. European Radiology 16, 1191–1205.

Harrigan, T.P., Jasty, M., Mann, R.W., Harris, W.H., 1988. Limitations of the continuum assumption in cancellous bone. Journal of Biomechanics 21, 269–275.

Harrigan, T.P., Mann, R.W., 1984. Characterization of microstructural anisotropy in orthotropic materials using a second rank tensor. Journal of Materials Science 19, 761–767.

Huiskes, R., 1993. Mechanical failure in total hip arthroplasty with cement. Current Orthopaedics 7, 239–247.

Huiskes, R., Chao, E.Y.S., 1983. A survey of finite element analysis in orthopedic biomechanics: the first decade. Journal of Biomechanics 16, 385–409.

Kabel, J., Odgaard, A., van Rietbergen, B., Huiskes, R., 1999a. Connectivity and the elastic properties of cancellous bone. Bone 24, 115–120.

Kabel, J., van Rietbergen, B., Odgaard, A., Huiskes, R., 1999b. Constitutive relationships of fabric, density, and elastic properties in cancellous bone architecture. Bone 25, 481–486.

Keller, T.S., 1994. Predicting the compressive mechanical behavior of bone. Journal of Biomechanics 27, 1159–1168.

Keyak, J.H., Fourkas, M.G., Meagher, J.M., Skinner, H.B., 1993. Validation of an automated method of three-dimensional finite element modelling of bone. Journal of Biomedical Engineering 15, 505–509.

Keyak, J.H., Lee, I.Y., Skinner, H.B., 1994. Correlations between orthogonal mechanical properties and density of trabecular bone: use of different densitometric measures. Journal of Biomedical Materials Research 28, 1329–1336.

Keyak, J.H., Rossi, S.A., Jones, K.A., Skinner, H.B., 1997. Prediction of femoral fracture load using automated finite element modeling. Journal of Biomechanics 31, 125–133.

Matsuura, M., Eckstein, F., Lochmuller, E.M., Zysset, P.K., 2008. The role of fabric in the quasi-static compressive mechanical properties of human trabecular bone from various anatomical locations. Biomechanics and Modeling in Mechanobiology 7, 27–42.

Morgan, E.F., Bayraktar, H.H., Keaveny, T.M., 2003. Trabecular bone modulus-density relationships depend on anatomic site. Journal of Biomechanics 36, 897–904.

Mulder, L., van Rietbergen, B., Noordhoek, N.J., Ito, K., 2012. Determination of vertebral and femoral trabecular morphology and stiffness using a flat-panel C-arm-based CT approach. Bone 50, 200–208.

Odgaard, A., 1997. Three-dimensional methods for quantification of cancellous bone architecture. Bone 20, 315–328.

Pahr, D.H., Zysset, P.K., 2009. A comparison of enhanced continuum FE with micro-FE models of human vertebral bodies. Journal of Biomechanics 42, 455–462.

Pettersen, S.H., Wik, T.S., Skallerud, B., 2009. Subject specific finite element analysis of stress shielding around a cementless femoral stem. Clinical Biomechanics 24, 196–202.

Rice, J.C., Cowin, S.C., Bowman, J.A., 1988. On the dependence of the elasticity and strength of cancellous bone on apparent density. Journal of Biomechanics 21, 155–168.

Rincon-Kohli, L., Zysset, P.K., 2009. Multi-axial mechanical properties of human trabecular bone. Biomechanics and Modeling in Mechanobiology 8, 195–208.

Tabor, Z., 2007. Estimating structural properties of trabecular bone from gray-level low-resolution images. Medical Engineering and Physics 29, 110–119.

Taddei, F., Cristofolini, L., Martelli, S., Gill, H.S., Viceconti, M., 2006. Subject-specific finite element models of long bones: an in-vitro evaluation of the overall accuracy. Journal of Biomechanics 39, 2457–2467.

Tawara, D., Sakamoto, J., Murakami, H., Kawahara, N., Oda, J., Tomita, K., 2010. Mechanical evaluation by patient-specific finite element analyses demonstrates therapeutic effects for osteoporotic vertebrae. Journal of the Mechanical Behavior of Biomedical Materials 3, 31–40.

Trabelsi, N., Yosibash, Z., Wutte, C., Augat, P., Eberle, S., 2011. Patient-specific finite element analysis of the human femur—a double-blinded biomechanical validation. Journal of Biomechanics 44, 1666–1672.

Turner, C.H., Cowin, S.C., Rho, J.Y., Ashman, R.B., Rice, J.C., 1990. The fabric dependence of the orthotropic elastic constants of cancellous bone. Journal of Biomechanics 23, 549–561.

van Rietbergen, B., Huiskes, R., Eckstein, F., Rüegsegger, P., 2003. Trabecular bone tissue strains in the healthy and osteoporotic human femur. Journal of Bone and Mineral Research 18, 1781–1788.

Verhulp, E., van Rietbergen, B., Huiskes, R., 2006. Comparison of micro-level and continuum-level voxel models of the proximal femur. Journal of Biomechanics 39, 2951–2957.

Verhulp, E., van Rietbergen, B., Huiskes, R., 2008. Load distribution in the healthy and osteoporotic human proximal femur during a fall to the side. Bone 42, 30–35.

Walsh, C.J., Phan, C.M., Misra, M., Bredella, M.A., Miller, K.K., Fazeli, P.K., Bayraktar, H.H., Klibanski, A., Gupta, R., 2010. Women with anorexia nervosa: finite element and trabecular structure analysis by using flat-panel volume CT. Radiology 257, 167–174.

Weinans, H., Sumner, D.R., Igloria, R., Natarajan, R.N., 2000. Sensitivity of periprosthetic stress-shielding to load and the bone density-modulus relationship in subject-specific finite element models. Journal of Biomechanics 33, 809–817.

Yang, G., Kabel, J., van Rietbergen, B., Odgaard, A., Huiskes, R., Cown, S., 1998. The anisotropic Hooke's law for cancellous bone and wood. Journal of Elasticity 53, 125–146.

Zysset, P.K., 2003. A review of morphology–elasticity relationships in human trabecular bone: theories and experiments. Journal of Biomechanics 36, 1469–1485.

Zysset, P.K., Curnier, A., 1995. An alternative model for anisotropic elasticity based on fabric tensors. Mechanics of Materials 21, 243–250.